Electronic Supplementary Material (ESI) for Journal of Materials Chemistry C.

Electronic Supplementary Information

A terbium(III) lanthanide–organic framework as a platform for recyclable multi-responsive luminescent sensor

Min Chen, Wen-Ming Xu, Jia-Yue Tian, Hui Cui, Jiao-Xing Zhang, Chun-Sen Liu* and Miao Du*

Henan Provincial Key Laboratory of Surface & Interface Science, Zhengzhou University of Light Industry, Zhengzhou 450002, China

* E-mail: chunsenliu@zzuli.edu.cn, dumiao@zzuli.edu.cn

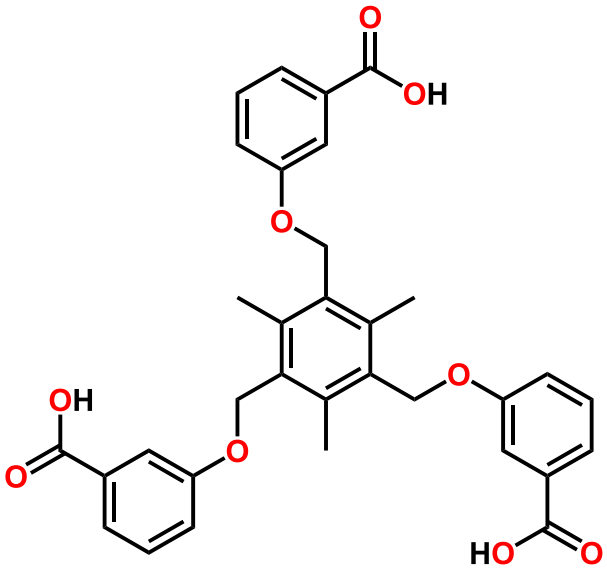

Scheme S1. Schematic drawing of the ligand H_3TBOT.

Table S1. Crystallographic data and structure refinement details for 534-MOF-Tb.

	534-MOF-Tb
Empirical formula	$C_{33}H_{29}O_{10}Tb$
Formula weight	744.48
Crystal system	Monoclinic
Space group	*C*2/c
a / Å	30.773(2)
b / Å	9.3088(4)
c / Å	30.411(2)
β / °	111.272(8)
Volume /Å^3	8118.2(9)
Z	8
D / g cm^{-3}	1.218
μ /mm^{-1}	8.940
F (000)	2976
R_{int}	0.0447
Goodness-of-fit on F^2	0.841
$R_1{}^a$ / $wR_2{}^b$ [$I > 2\sigma(I)$]	0.0935 / 0.2304
$R_1{}^a$ / $wR_2{}^b$ (All data)	0.1023 / 0.2403
CCDC number	1509860

[a] $R_1 = \Sigma||F_o| - |F_c||/\Sigma|F_o|$. [b] $wR_2 = |\Sigma w(|F_o|^2 - |F_c|^2)|/\Sigma|w(F_o)^2|^{1/2}$, where $w = 1/[\sigma^2(F_o^2) + (aP)^2 + bP]$. $P = (F_o^2 + 2F_c^2)/3$.

Table S2. A comparison of the selected bond lengths (Å) and angles (°) for 534-MOF-Tb.[a]

534-MOF-Tb			
Tb1–O1	2.272(6)	Tb1–O10	2.452(8)
Tb1–O2$^{\#1}$	2.294(6)	Tb1–O6$^{\#2}$	2.323(7)
Tb1–O5$^{\#3}$	2.354(6)	Tb1–O4$^{\#4}$	2.376(6)
Tb1–O3$^{\#5}$	2.377(6)	Tb1–O4$^{\#5}$	2.713(7)
O1–Tb1–O2$^{\#1}$	80.8(2)	O1–Tb1–O6$^{\#2}$	93.8(3)
O2$^{\#1}$–Tb1–O6$^{\#2}$	145.6(2)	O1–Tb1–O5$^{\#3}$	111.9(3)
O2$^{\#1}$–Tb1–O5$^{\#3}$	77.2(2)	O6$^{\#2}$–Tb1–O5$^{\#3}$	134.9(2)
O1–Tb1–O4$^{\#4}$	83.1(3)	O2$^{\#1}$–Tb1–O4$^{\#4}$	139.7(2)
O6$^{\#2}$–Tb1–O4$^{\#4}$	72.0(2)	O5$^{\#3}$–Tb1–O4$^{\#4}$	75.0(2)
O1–Tb1–O3$^{\#5}$	149.4(3)	O2$^{\#1}$–Tb1–O3$^{\#5}$	80.6(2)
O6$^{\#2}$–Tb1–O3$^{\#5}$	88.0(3)	O5$^{\#3}$–Tb1–O3$^{\#5}$	87.3(3)
O4$^{\#4}$–Tb1–O3$^{\#5}$	126.1(2)	O1–Tb1–O10	75.8(4)
O2$^{\#1}$–Tb1–O10	73.3(3)	O6$^{\#2}$–Tb1–O10	72.5(3)
O5$^{\#3}$–Tb1–O10	147.8(3)	O4$^{\#4}$–Tb1–O10	136.9(3)
O3$^{\#5}$–Tb1–O10	75.7(3)	O1–Tb1–O4$^{\#5}$	157.3(2)
O2$^{\#1}$–Tb1–O4$^{\#5}$	121.05(19)	O6$^{\#2}$–Tb1–O4$^{\#5}$	71.7(2)
O5$^{\#3}$–Tb1–O4$^{\#5}$	71.1(2)	O4$^{\#4}$–Tb1–O4$^{\#5}$	75.9(2)
O3$^{\#5}$–Tb1–O4$^{\#5}$	50.2(2)	O10–Tb1–O4$^{\#5}$	114.4(3)

[a] Symmetry code: For 534-MOF-Tb and : #1 = $–x + 1/2, –y + 1/2, –z + 1$; #2 = $–x + 1, –y + 1, –z + 1$; #3 = $x – 1/2, y – 3/2, z$; #4 = $–x + 1, y – 1, –z + 3/2$; #5 = $x – 1/2, –y + 1/2, z – 1/2$.

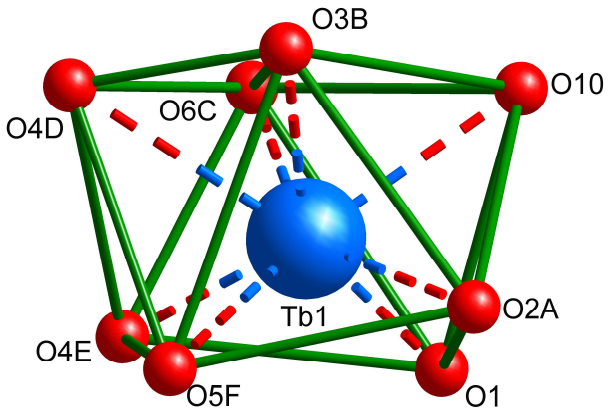

Fig. S1 Coordination sphere of the Tb^{3+} ion in 534-MOF-Tb. Symmetry codes = –*x* + 1/2, –*y* + 1/2, –*z* + 1 for A; *x* – 1/2, –*y* + 1/2, *z* – 1/2 for B; –*x* + 1, –*y* + 1, –*z* + 1 for C; *x* – 1/2, –*y* + 1/2, *z* – 1/2 for D; –*x* + 1, *y* – 1, –*z* + 3/2 for E; *x* – 1/2, *y* – 3/2, *z* for F.

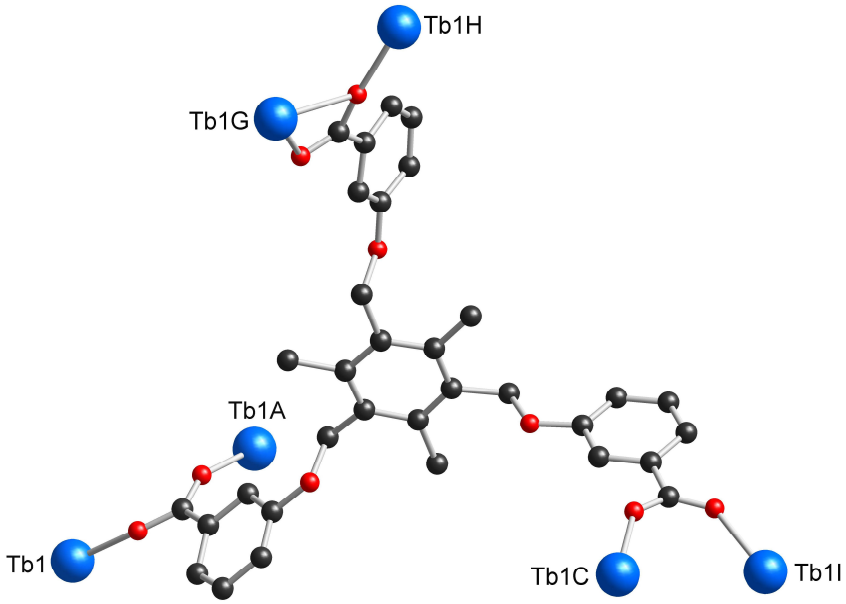

Fig. S2 Coordination mode of the TBOT ligand in 534-MOF-Tb. Symmetry codes = –*x* + 1/2, –*y* + 1/2, –*z* + 1 for A; –*x* + 1, –*y* + 1, –*z* + 1 for C; *x* + 1/2, –*y* + 1/2, *z* + 1/2 for G; –*x* + 1, *y* + 1, –*z* + 3/2 for H; *x* + 1/2, *y* + 3/2, *z* for I.

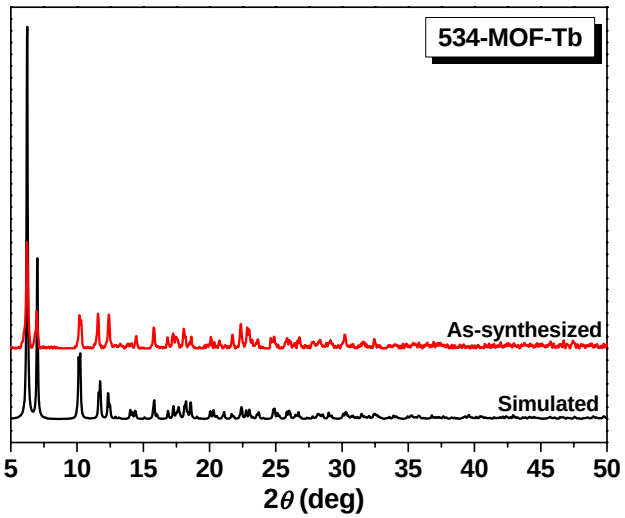

(a)

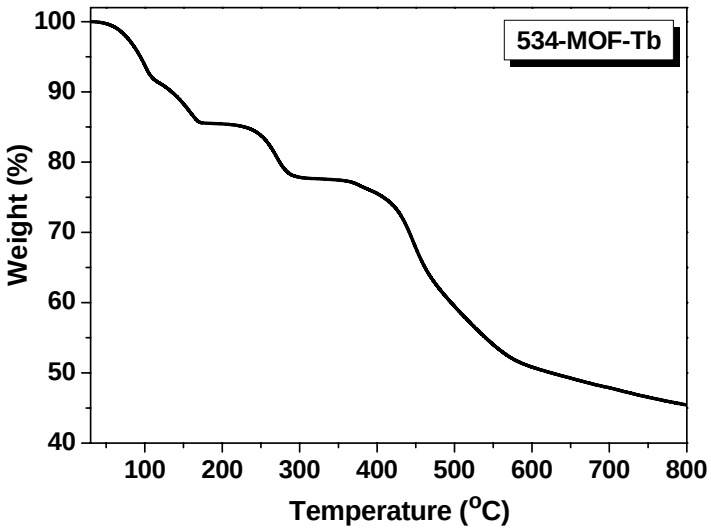

(b)

Fig. S3 Power X-ray diffraction patterns (a) and TGA curve (b) of 534-MOF-Tb.

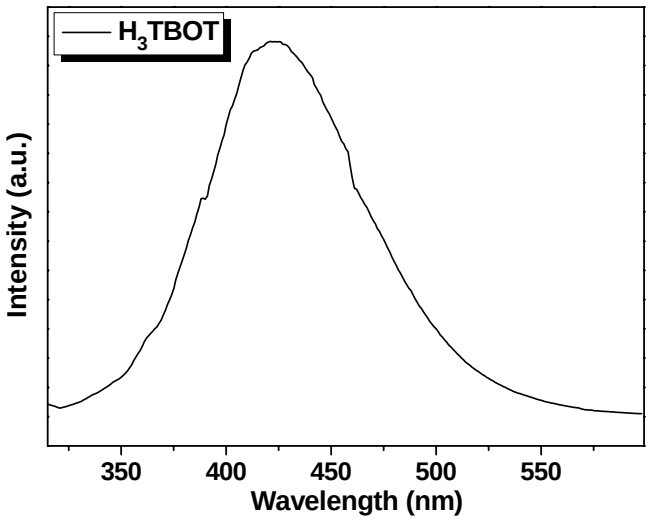

(a)

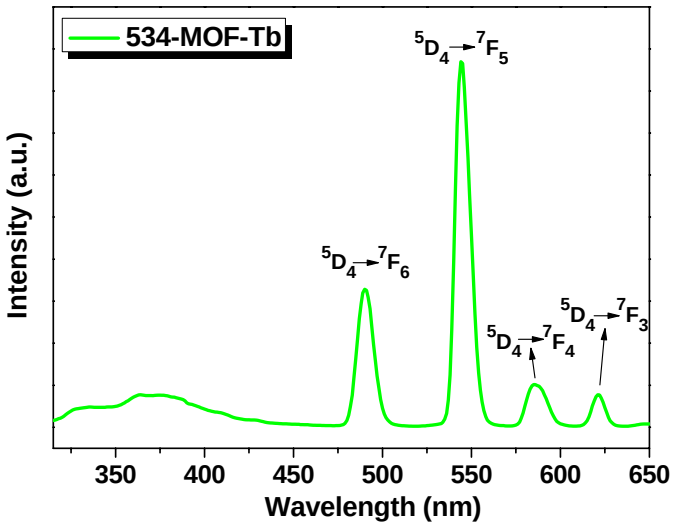

(b)

Fig. S4 Solid state emission spectra of H_3TBOT (a) and 534-MOF-Tb (b).

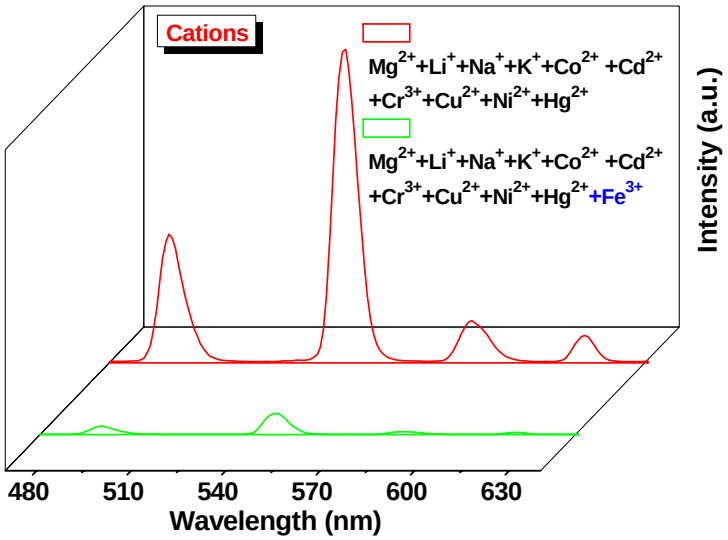

Fig. S5 Emission spectra of 534-MOF-Tb dispersed in aqueous solutions of mixed cations without or with Fe^{3+}.

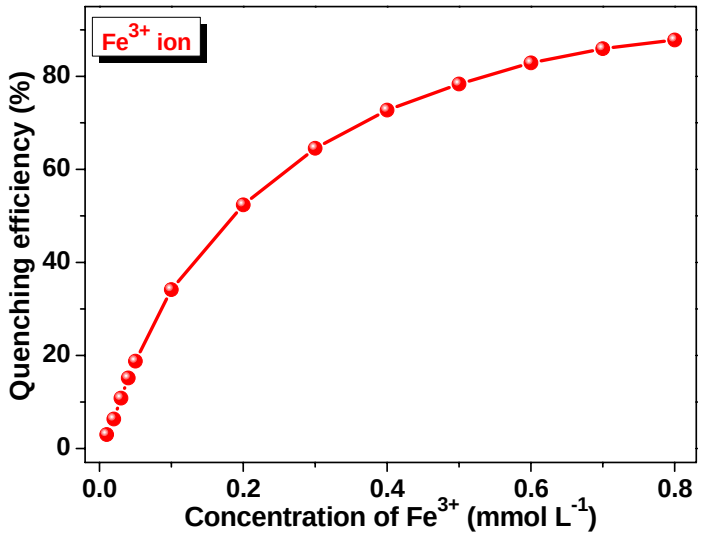

Fig. S6 Dependence of the quenching efficiency on the concentration of Fe^{3+}.

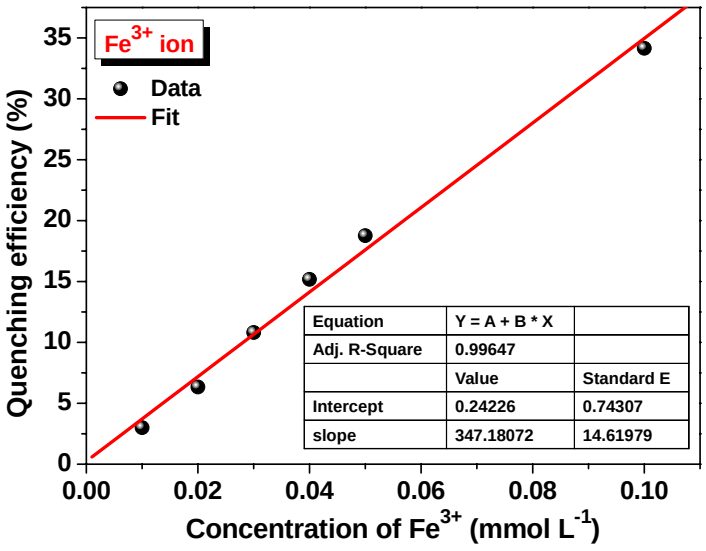

Fig. S7 The fitting plot of the quenching efficiency with the increasing concentration of Fe^{3+} in the low concentration range. The red line corresponds to a fit to the linear relationship.

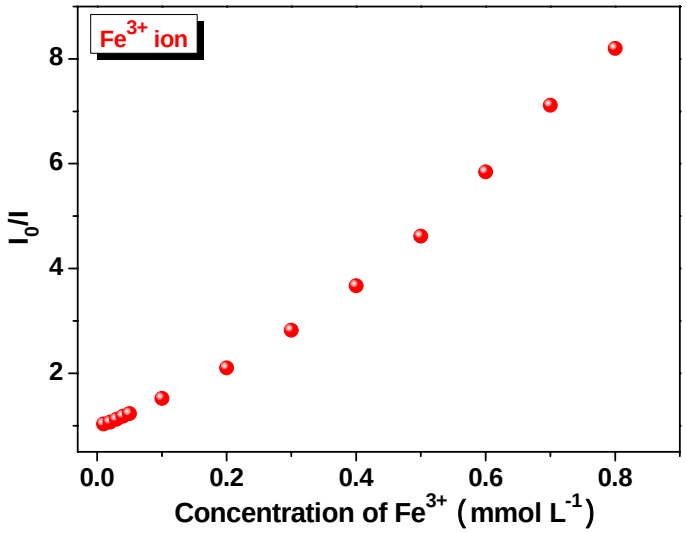

(a)

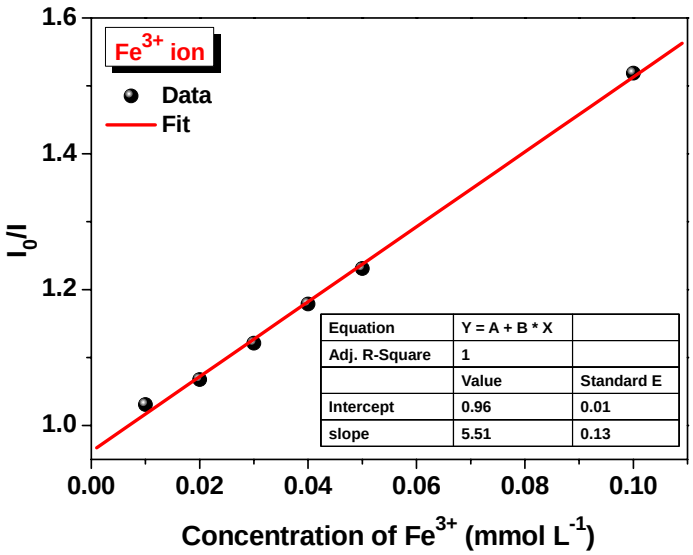

(b)

Fig. S8 (a) Stern–Volmer plot of I_0/I versus the concentration of Fe^{3+}. (b) The linear Stern–Volmer plot in the low concentration range. The red line corresponds to a fit to the linear relationship.

Table S3. A comparison between MOF-based luminescent probes for the detection of Fe^{3+}, $Cr_2O_7^{2-}$ and MnO_4^-.

Analyte	MOF	Solution	Detection Limit	K_{sv}	Ref.
Fe^{3+}	$[Tb(L_1)_{1.5}(H_2O)](H_2O)_3$	water	—	—	S1
Fe^{3+}	$[Eu(HL_2)(DMF)(H_2O)_2](H_2O)_3$	water	—	1.52×10^3	S2
Fe^{3+}	$[Tb(HL_2)(DMF)(H_2O)_2](H_2O)_3$	water	—	4.48×10^3	S2
Fe^{3+}	$[Zn_3(HL_2)_2(H_2O)_2](DMF)_2(H_2O)_7$	water	—	381.85	S2
Fe^{3+}	$[H_2NMe_2][Eu(HL_3)]$	water	—	—	S3
Fe^{3+}	$([Eu_2(L_4)_3(DMA)(H_2O)_3](DMA)(H_2O)_{4.5}$	water	—	1.07×10^4	S4
Fe^{3+}	$[Eu(HL_5)_2(NO_3)](H_2O)$	ethanol	0.026 mmol L^{-1}	—	S5
$Cr_2O_7^{2-}$	$[Eu(HL_5)_2(NO_3)](H_2O)$	ethanol	0.022 mmol L^{-1}	—	S5
$Cr_2O_7^{2-}$	$[Zn(L_6)(L_7)]$	water	—	6.56×10^6	S6
MnO_4^-	$[Ba_3La_{0.5}(\mu_3\text{-}L_8)_{2.5}(H_2O)_3(DMF)](DMF)_3$	water	0.28 μM	7.73×10^3	S7

H_2L_1 = 2-(2-hydroxy-propionylamino)-terephthalic acid;

H_4L_2 = 2,8,14,20-tetra-ethyl-6,12,18,24-tetra-methoxy-4,10,16,22-tetra-carboxy-methoxy-calix[4]arene);

H_4L_3 = tetrakis[4-(carboxyphenyl)oxamethyl]methane acid;

H_2L_4 = 9,9-dimethyl-2,7-fluorenedicarboxylic acid;

H_2L_5 = 3-(1*H*-pyrazol-3-yl) benzoic acid;

HL_6 = 2-amino-1,4-benzenedicarboxylic acid;

L_7 = 4,4′-bis(imidazol-1-ylmethyl)-biphenyl;

H_3L_8 = *p*-terphenyl-3,4″,5-tricarboxylic acid;

DMF = dimethylformamide;

DMA = dimethylacetamide.

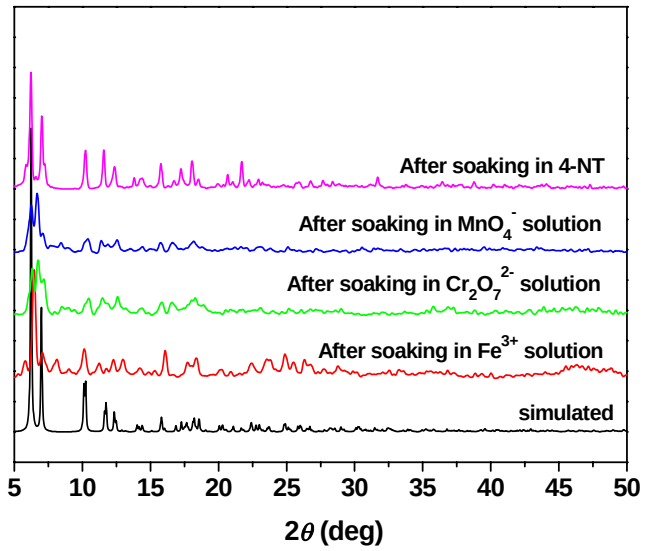

Fig. S9 Power X-ray diffraction patterns of 534-MOF-Tb after five recyclable experiments.

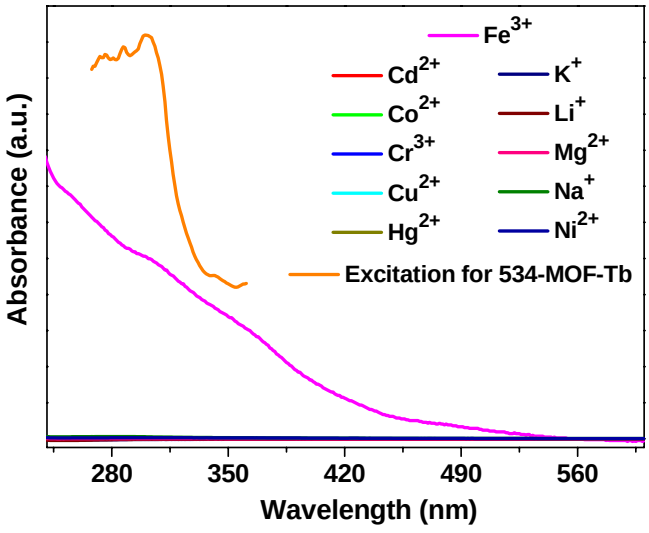

Fig. S10 The UV–Vis absorption spectrum of aqueous solutions of different testing cations (Li^+, Na^+, K^+, Mg^{2+}, Cu^{2+}, Co^{2+}, Cd^{2+}, Ni^{2+}, Hg^{2+}, Cr^{3+}, and Fe^{3+}) and the excitation for 534-MOF-Tb.

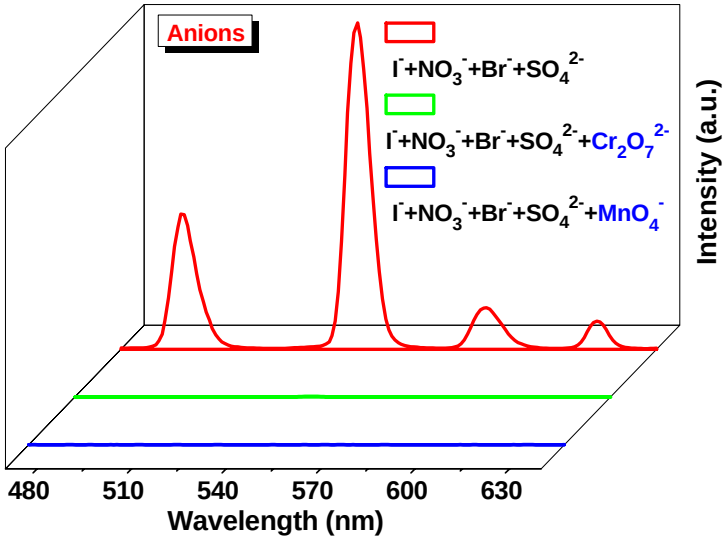

Fig. S11 Emission spectra of 534-MOF-Tb soaking in mixed anions aqueous solutions without or with $Cr_2O_7^{2-}$ or MnO_4^-.

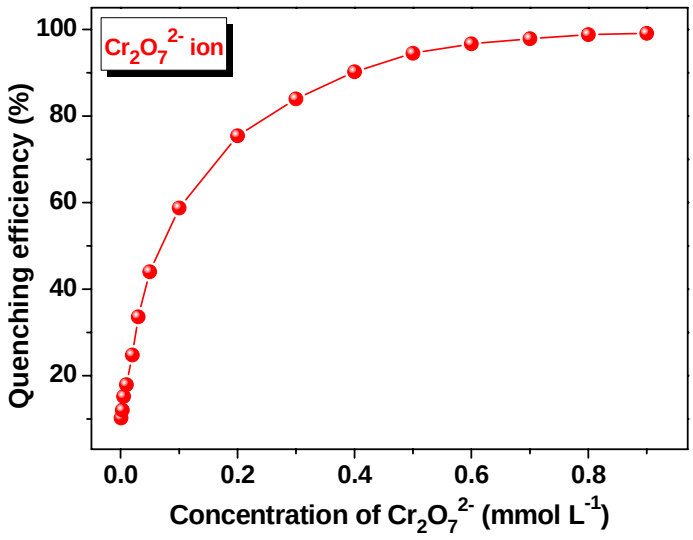

(a)

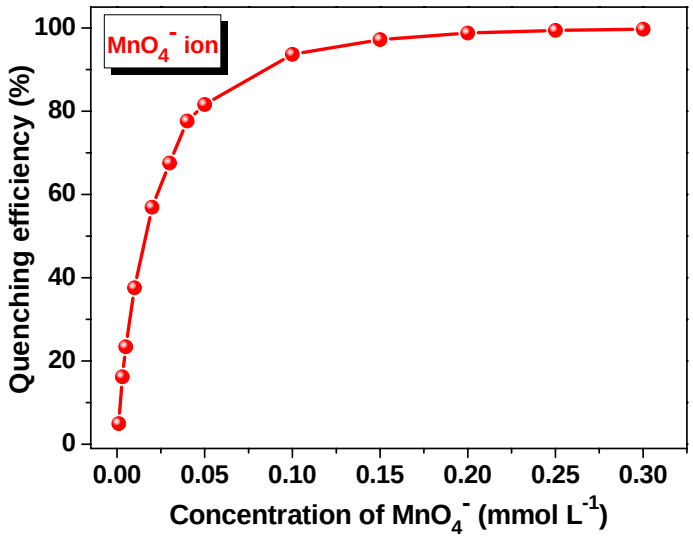

(b)

Fig. S12 Dependence of the quenching efficiencies on the concentration of $Cr_2O_7^{2-}$ (a) and MnO_4^- (b).

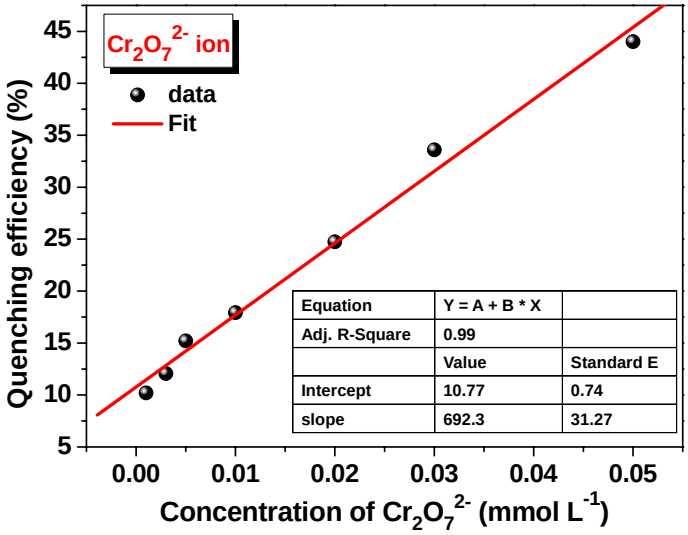

(a)

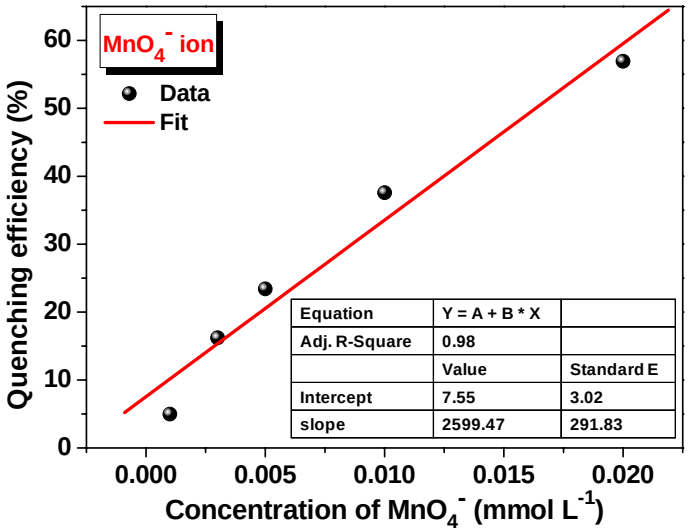

(b)

Fig. S13 The fitting plot of the quenching efficiencies with the increasing concentration of $Cr_2O_7^{2-}$ (a) and MnO_4^- (b) in the low concentration range. The red line corresponds to a fit to the linear relationship.

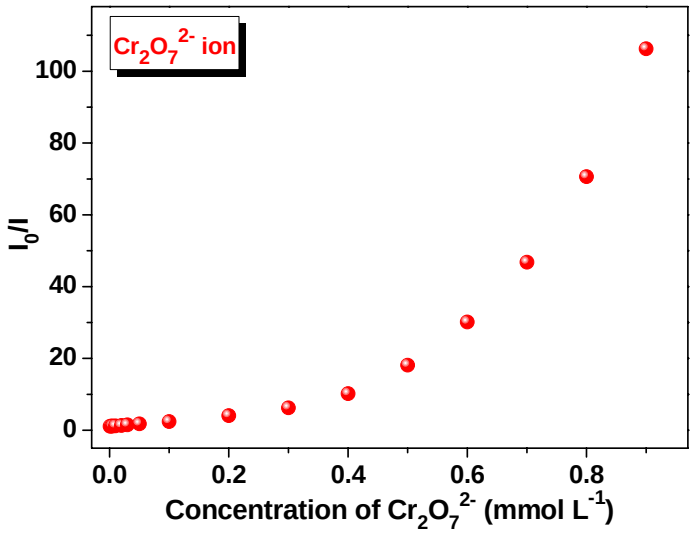

(a)

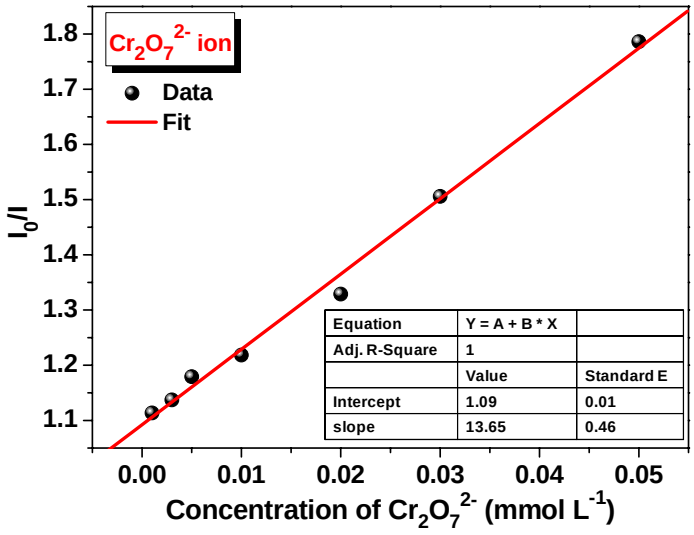

(b)

Fig. S14 (a) Stern–Volmer plot of I_0/I versus the concentration of $Cr_2O_7^{2-}$. (b) The linear Stern–Volmer plot in the low concentration range. The red line corresponds to a fit to the linear relationship.

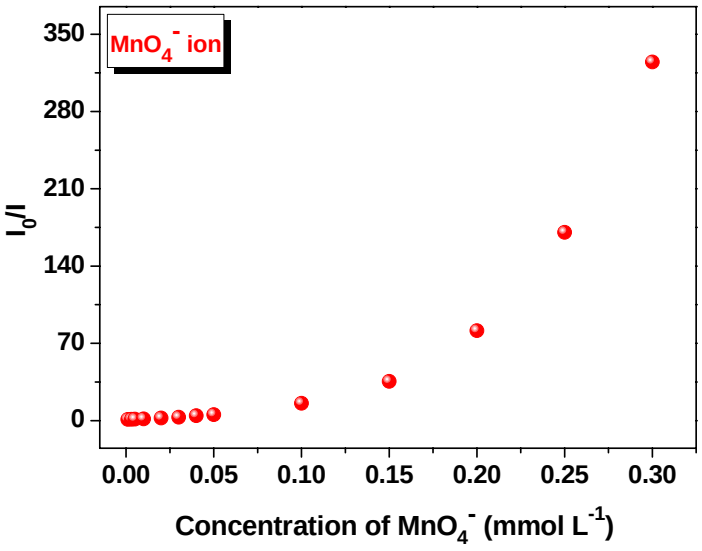

(a)

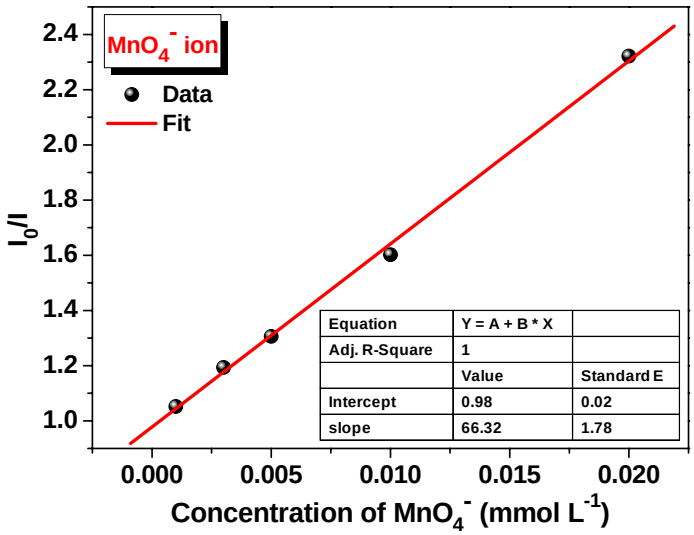

(b)

Fig. S15 (a) Stern–Volmer plot of I_0/I versus the concentration of MnO_4^-. (b) The linear Stern–Volmer plot in the low concentration range. The red line corresponds to a fit to the linear relationship.

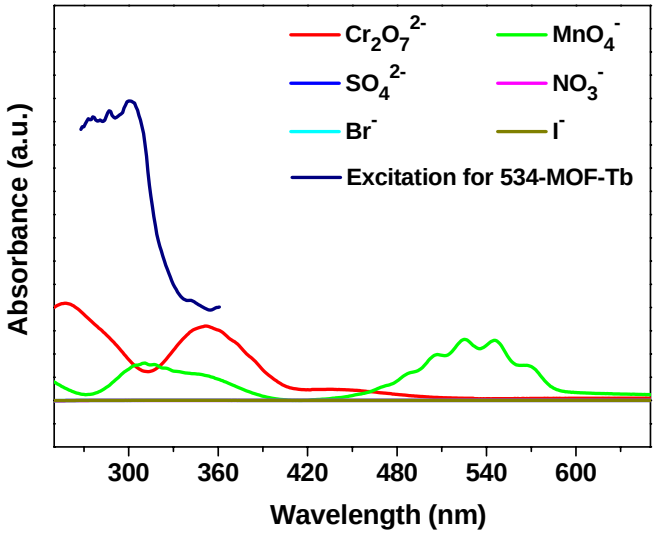

Fig. S16 The UV–Vis absorption spectra of aqueous solutions of testing anions (Br^-, I^-, NO_3^-, SO_4^{2-}, MnO_4^-, and $Cr_2O_7^{2-}$) and the excitation for 534-MOF-Tb.

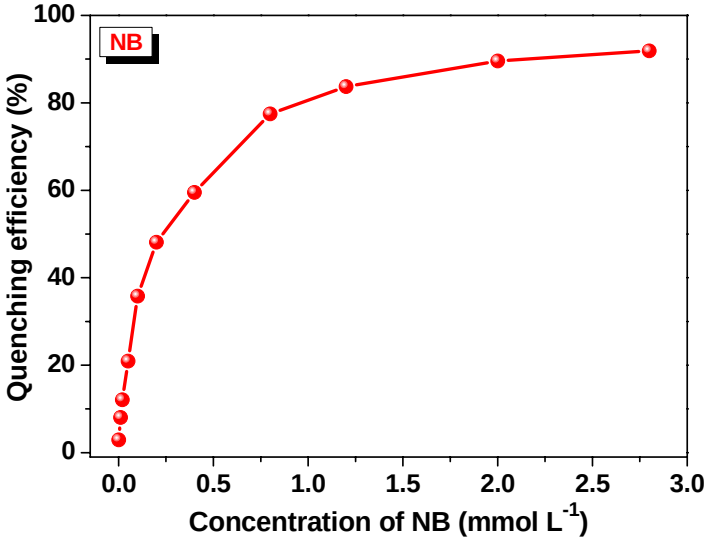

(a)

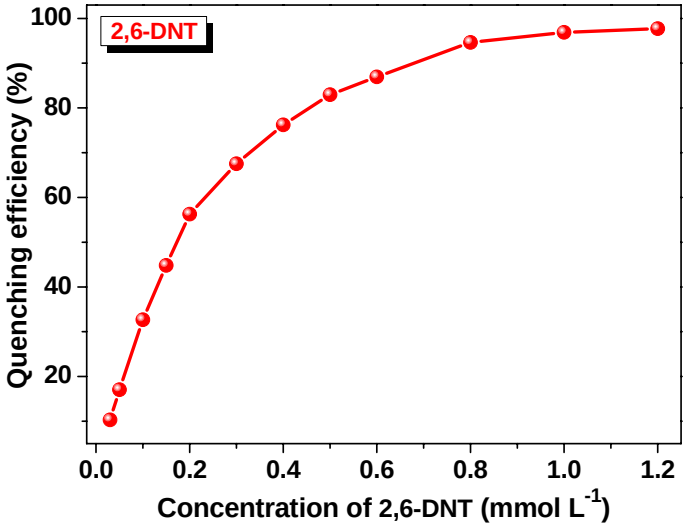

(b)

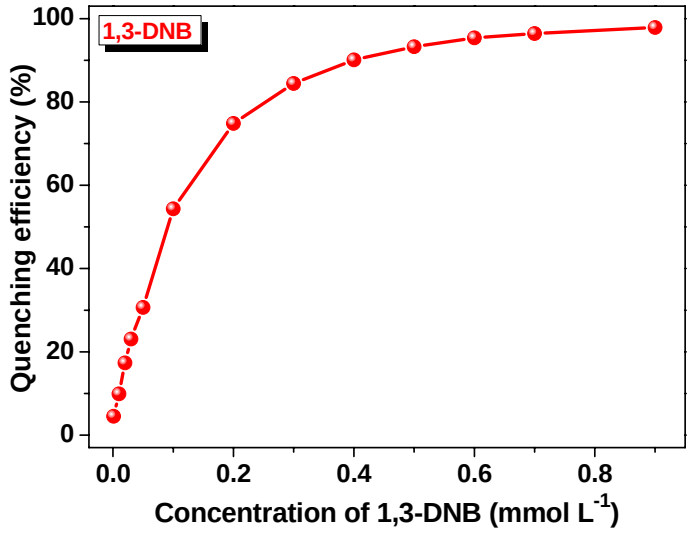

(c)

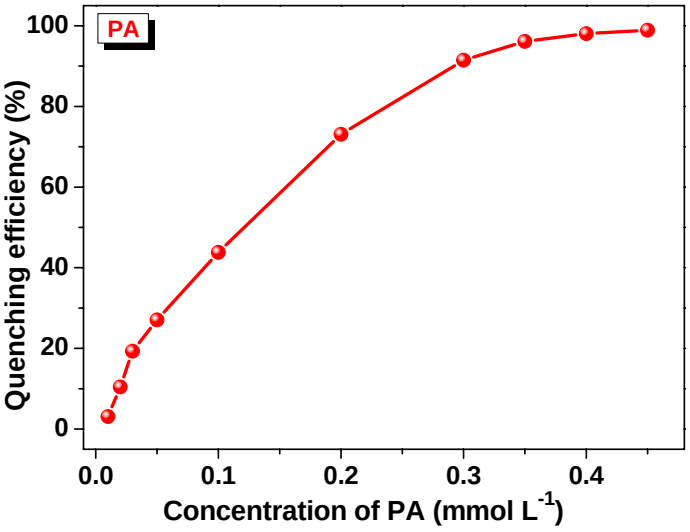

(d)

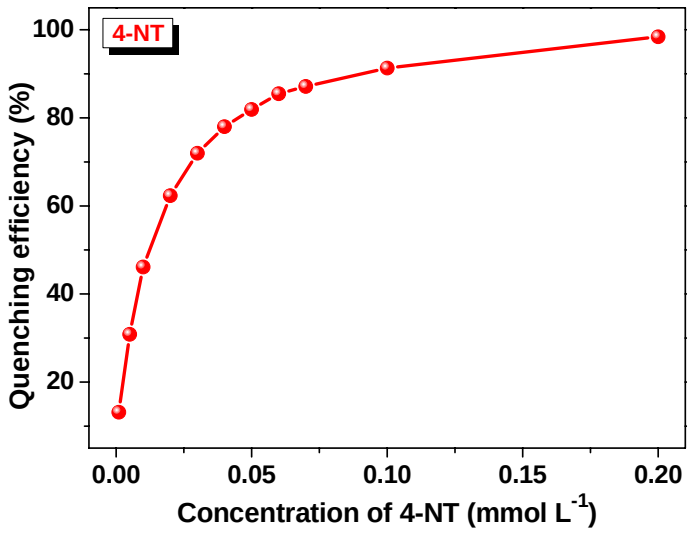

(e)

Fig. S17 Dependence of the quenching efficiencies on the concentration of NB (a), 2,6-DNT (b), 1,3-DNB (c), PA (d), and 4-NT (e).

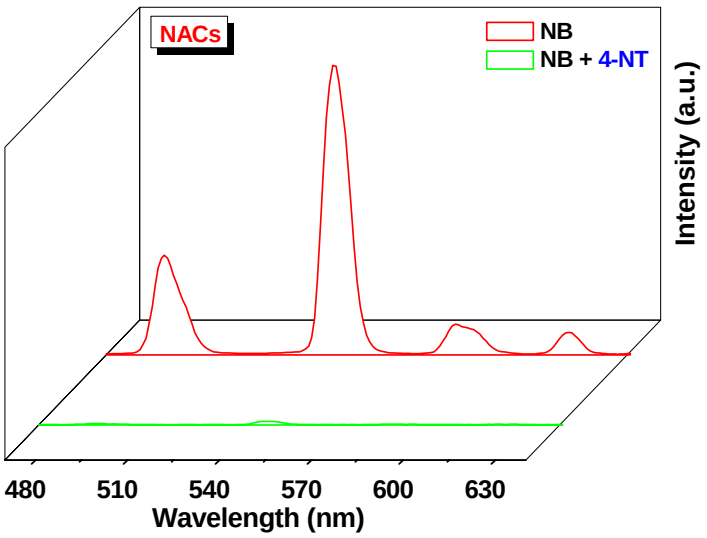

(a)

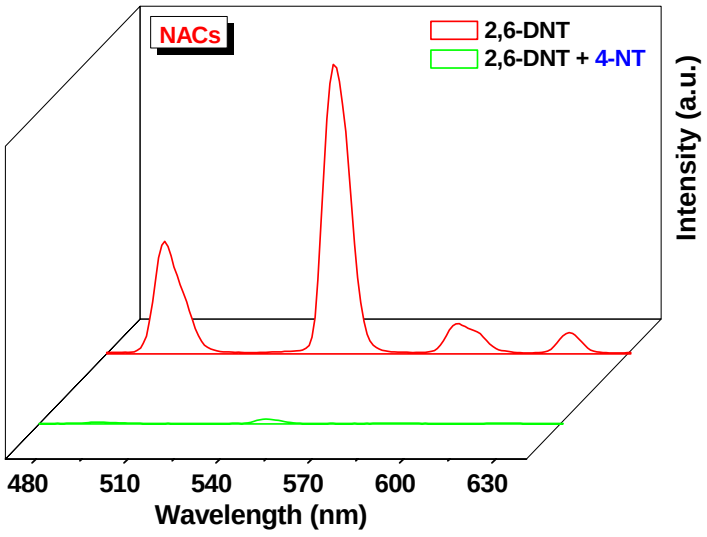

(b)

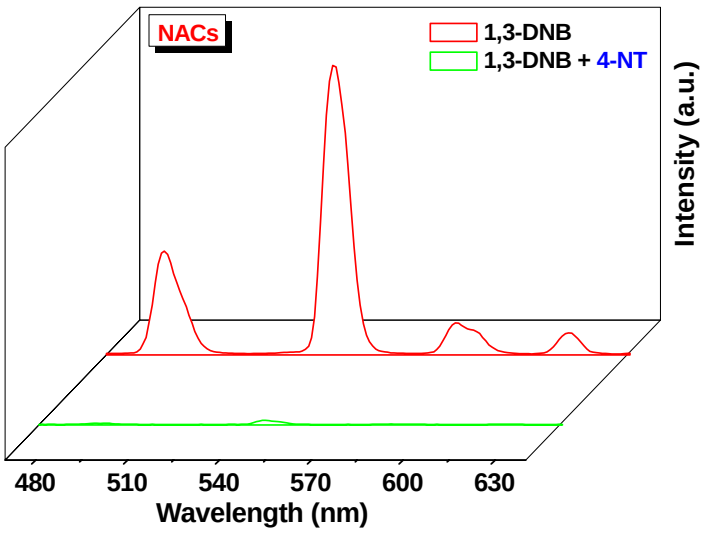

(c)

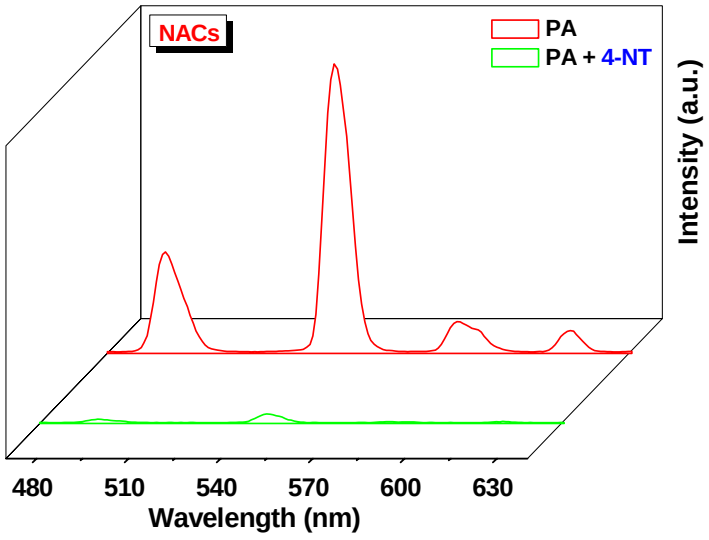

(d)

Fig. S18 Emission spectra of 534-MOF-Tb soaking in the single and mixed NACs DMF solutions with 4-NT.

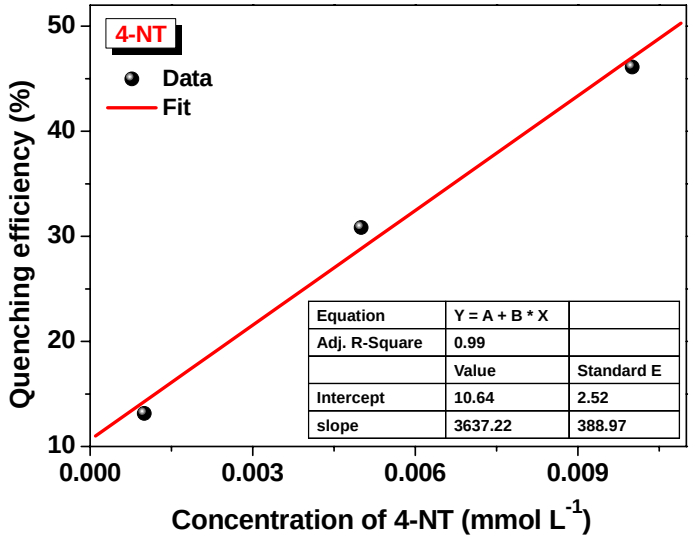

Fig. S19 The fitting plot of the quenching efficiency with the increasing concentration of 4-NT in the low concentration range. The red line corresponds to a fit to the linear relationship.

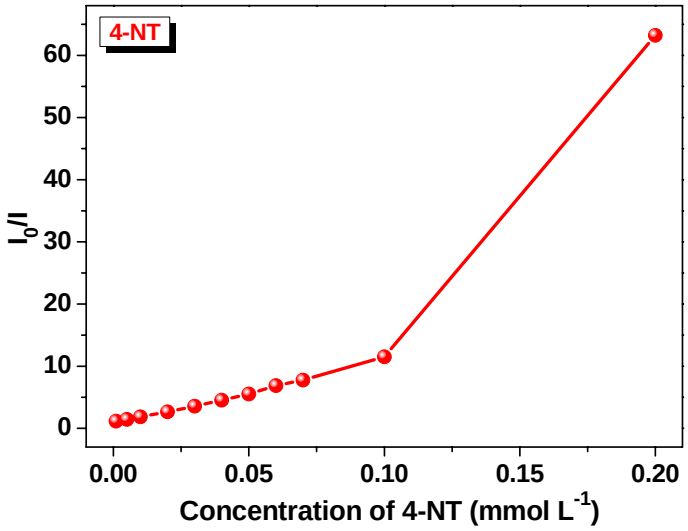

(a)

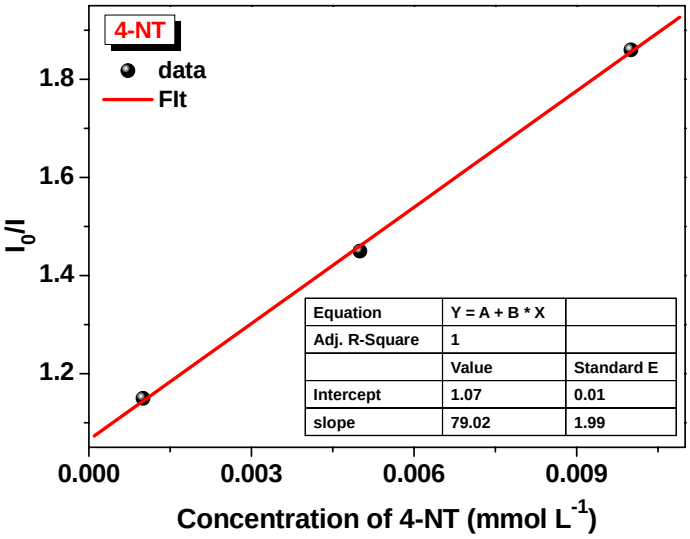

(b)

Fig. S20 (a) Stern–Volmer plot of I_0/I versus the concentration of 4-NT. (b) The linear Stern–Volmer plot in the low concentration range. The red line corresponds to a fit to the linear relationship.

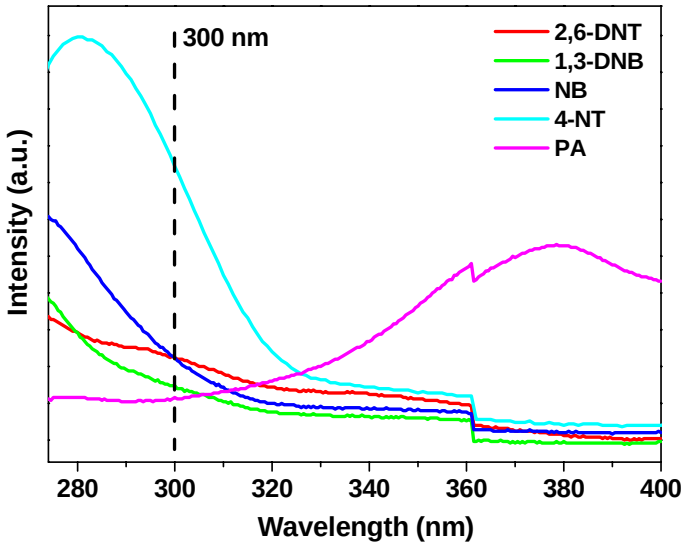

Fig. S21 UV-Vis absorption spectra of the solutions of different NACs with the same concentration of 200 ppm.

References

S1 L.-H. Cao, F. Shi, W.-M. Zhang, S.-Q. Zang and T. C. W. Mak, *Chem. Eur. J.*, 2015, **21**, 15705.

S2 S.-T. Zhang, J. Yang, H. Wu, Y.-Y. Liu and J.-F. Ma, *Chem. Eur. J.*, 2015, **21**, 15806.

S3 S. Dang, E. Ma, Z.-M. Sun and H. Zhang, *J. Mater. Chem.*, 2012, **22**, 16920.

S4 L. Li, Q. Chen, Z. Niu, X. Zhou, T. Yang and W. Huang, *J. Mater. Chem. C*, 2016, **4**, 1900.

S5 G.-P. Li, G. Liu, Y.-Z. Li, L. Hou, Y.-Y. Wang and Z. Zhu, *Inorg. Chem.*, 2016, **55**, 3952**.**

S6 L. Wen, X. Zheng, K. Lv, C. Wang and X. Xu, *Inorg. Chem.*, 2015, **54**, 7133.

S7 B. Ding, S. X. Liu, Y. Cheng, C. Guo, X. X. Wu, J. H. Guo, Y. Y. Liu and Y. Li, *Inorg. Chem.*, 2016, **55**, 4391.